Top Catal (2016) 59:469–477
DOI 10.1007/s11244-015-0528-0

ORIGINAL PAPER

Are Au Nanoparticles on Oxygen-Free Supports Catalytically Active?

Alexander Yu. Klyushin[1] · Rosa Arrigo[1] · Yi Youngmi[1] · Zailai Xie[1] · Michael Hävecker[1,2] · Andrey V. Bukhtiyarov[3,4] · Igor P. Prosvirin[3,4] · Valerii I. Bukhtiyarov[3,4] · Axel Knop-Gericke[1] · Robert Schlögl[1]

Published online: 11 January 2016

Abstract Gold nanoparticles (Au NPs) on oxygen-free supports were examined using near ambient pressure X-ray photoelectron spectroscopy under CO oxidation conditions, and ex situ using scanning electron microscopy and transmission electron microscopy. Our observations demonstrate that Au NPs supported on carbon materials are inactive, regardless of the preparation method. Ozone (O_3) treatment of carbon supports leads oxygen-functionalization of the supports. When subsequently exposed to a CO feed, CO is oxidized by the functionalized sites of the carbon support via a stoichiometric pathway. Microscopy reveals that the reaction with CO does not change the morphology of the Au NPs. In situ XPS reveals that the O_3 treatment gives rise to additional Au 4f and O 1s peaks at binding energies of 85.25–85.6 and 529.4–530 eV, respectively, which are assigned to the presence of Au oxide. A surface oxide phase is formed during the activation of Au NPs supported on Au foil by O_3 treatment. However, this phase decomposes in vacuum and the remaining low-coordinative atoms do not have sufficient catalytic properties to oxidize CO, so the size reduction of Au NPs and/or oxidation of Au NPs is not sufficient to activate Au.

Keywords Gold nanoparticles · Gold oxide · X-ray photoemission spectra · Surface core-level shift · CO oxidation · Strong metal-support interaction

1 Introduction

Gold-based catalysts have attracted a lot of interest since Haruta's study [1, 2]. Au catalytic systems demonstrate high activity in many application, in particular in complete [3, 4], selective [5, 6] and partial [3, 7] oxidation reactions. The number of publications on the application of Au in catalysis increases each year; however, the mechanism of the reactions is still debated in the literature.

The complexity of Au-containing catalysts suggests many possible factors may influence the catalytic activity of gold, such as particle size and shape, the support morphology and nature, activation (pre-)treatment, presence of adsorbed oxygen or water etc. In the literature, there is no consensus about active species; some authors consider metallic gold [8, 9] as active sites, while others suggest positive (δ+) [10, 11] and negative (δ−) [12, 13] low-charged gold or oxidized (1+, 3+) states [14]. Identification of active sites requires a systematic study of Au-based catalysts, by varying one or few parameters. One of the potentially most important parameters is the support. Therefore we divide Au catalytic systems into two broad groups: Au on oxygen-free supports and Au on oxides.

Here, we present a study of Au catalysts on oxygen-free supports in the CO oxidation reaction, using a combination

Electronic supplementary material The online version of this article (doi:10.1007/s11244-015-0528-0) contains supplementary material, which is available to authorized users.

✉ Alexander Yu. Klyushin
klyushin@fhi-berlin.mpg.de

[1] Fritz-Haber-Institute der Max Planck Society, Faradayweg 4-6, 14195 Berlin, Germany

[2] Division Solar Energy Research, Helmholtz-Zentrum Berlin für Materialien und Energie GmbH, Albert-Einstein-Str. 15, 12489 Berlin, Germany

[3] Boreskov Institute of Catalysis, Pr. Lavrentieva 5, Novosibirsk 630090, Russia

[4] Novosibirsk State University, Piragova str. 2, Novosibirsk 630090, Russia

of in situ XPS and ex situ transmission electron microscopy (TEM) and scanning electron microscopy (SEM). Near ambient pressure X-ray photoelectron spectroscopy (NAP-XPS) measurements allow us to characterize the electronic structure of nanoscopic Au and support, while microscopy provides information about morphology of Au NPs before and after reaction. The combination of these techniques helps one to understand the origin of Au catalytic activity and clarify the mechanism of the reaction.

2 Materials

2.1 Au/HOPG

Model Au/HOPG catalysts were prepared inside a preparation chamber attached to a photoelectron spectrometer (Novosibirsk, Russia) which was built by SPECS (Germany). The analyzer chamber was equipped with a hemispherical analyzer PHOIBOS-150-MCD-9, an ellipsoidal monochromator FOCUS 500 and an X-ray source XR 50 M with double Al/Ag anode. The three-step preparation procedure, previously used to prepare Ag/HOPG (highly oriented pyrolytic graphite) model catalysts, as described in detail elsewhere [15], was used to prepare Au/HOPG model catalysts. This procedure consists of an initial stage of defect formation on the HOPG surface by soft Ar^+ sputtering followed by Au deposition and surface annealing at T = 300 °C in UHV (for Au NPs stabilization). The Au nanoparticle size was varied by changing the amount of deposited gold, which was controlled by monitoring the ratio of Au 4f to C 1s XPS peak areas, a final Au load was 1 wt%.

2.2 Au/N-CNTs

Multi-walled carbon nanotubes were supplied by Applied Science ltd. 20 g CNTs were treated with 1 L of concentrated HNO_3 under reflux for 4 h. Then the nanotubes were filtrated and washed with distilled water until the filtrate showed a neutral pH. Subsequently, the sample was dried at 110 °C for 3 d in air. N-functionalized CNTs (N-CNTs) were obtained via a treatment of the previously oxidized nanotubes with NH_3 at 700 °C for 6 h. For this purpose 3 g of the material were placed in a quartz tube under a flow of 120 mL/min composed of 10 % NH_3 in Ar.

5 mg of NaN_3 were dissolved in 10 mL of MilliQ water. Then 6 mg of trihydrate chloroauric acid ($HAuCl_4{\cdot}3H_2O$) were added to the solution, which subsequently turned orange. The ratio $NaN_3/HAuCl_4{\cdot}3H_2O$ was 5:1. 300 mg of N-CNTs were added to the solution in order to allow the adsorption of the Au precursor on the N-CNTs with a final Au load of 1wt%. The addition of the N-CNTs induced gas release and caused the solution to turn colorless, indicating the decomposition and complete adsorption of the precursor. Afterwards, the N-CNT suspension was filtered and the total precursor decomposition was ensured by photo-treatment with an UV/Vis lamp for 30 min.

2.3 Au/O-CNTs

10 g Baytubes C150HP were treated with 500 mL of 3 molar HNO_3 [diluted with water from nitric acid 65 % (Merck)] at room temperature (RT) for 24 h. Then the O-functionalized CNTs (O-CNTs) were thoroughly washed and filtrated with Millipore water until a neutral pH was obtained. For the synthesis of Au/O-CNT, 1 g of O-CNTs was impregnated with 6 mL aqueous solution containing 20.2 mg of $HAuCl_4$. The slurry was then sonicated in an ultrasonic bath for 10 s and afterwards the solvent was evaporated slowly at RT in air for 48 h. Thereafter, the samples containing the metal precursor were reduced in 20 % H_2/Ar gas mixture at 250 °C for 2 h, a final Au load was 1 wt%.

2.4 Au/Au Foil

Au nanoparticles on Au foil were prepared by electrodeposition. Electrochemical deposition was performed in a conventional three-electrode electrochemical cell using a potentiostat/galvanostat (VSP, Biologic). Au foil was used as the working electrode and Pt wire and saturated calomel electrode (SCE) were employed as the counter electrode and the reference electrode. Au electrolyte solution consisted of 0.1 mM $HAuCl_4$ + 0.1 M HCl. Au nanoparticles were then electrodeposited under a current potential of −0.4 V versus SCE for 60 s.

3 Methods

3.1 XPS

The NAP-XPS experiments were performed at the ISISS beamline of BESSY II/HZB (Berlin, Germany). All measurements were carried out in a stainless steel NAP-XPS chamber, the details of which are described elsewhere [16, 17]. The powder samples were pressed into a pellet of 8 mm diameter. Samples were placed between a stainless steel backplate and lid (with 6 mm hole) and mounted onto a sapphire sample holder. The samples were heated from the backside using an infrared laser and the temperature

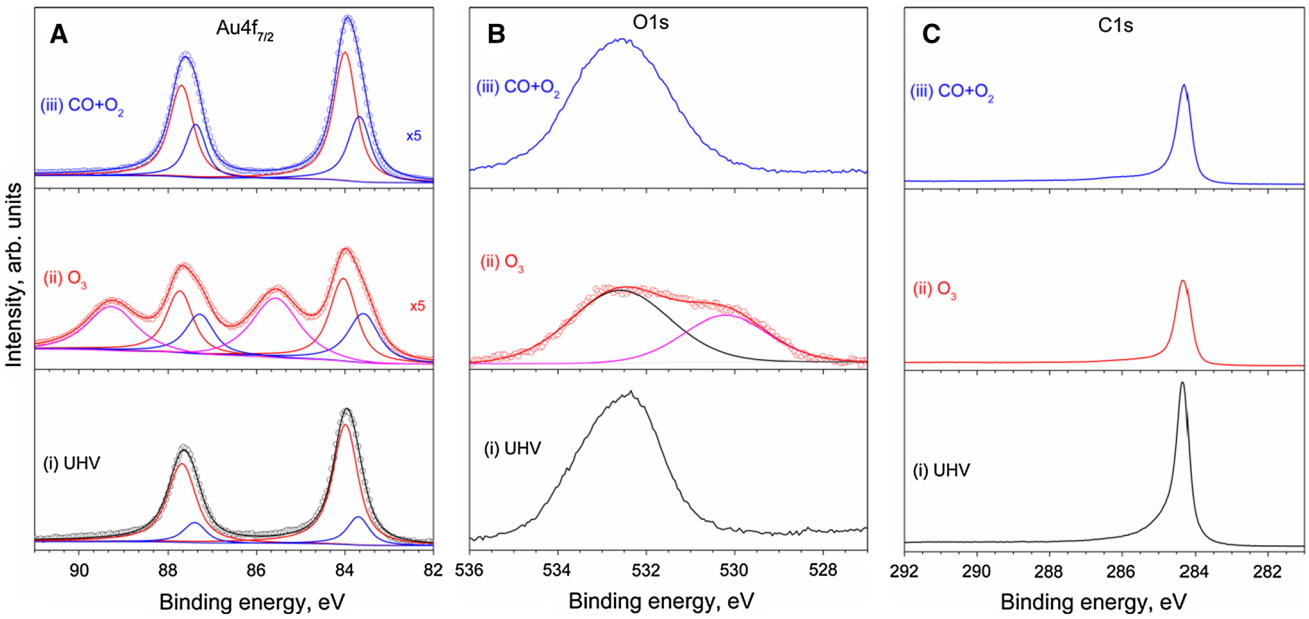

Fig. 1 NAP **a** Au 4f, **b** O 1s and **c** C 1s XP spectra of Au/HOPG (*i*) in UHV at RT, (*ii*) under O_3 at $p = 0.3$ mbar, T = 100 °C and (*iii*) under CO and O_2 atmosphere at $p = 0.3$ mbar, RT. Photoelectrons with 150 eV kinetic energy were used to collect surface sensitive Au 4f, O 1s and C 1s spectra in UHV and CO + O_2, and photons with 720 eV energy were used to collect Au 4f, O 1s and C 1s spectra during O_3 treatment

was measured by a thermocouple fastened to the sample surface. The overall spectral resolution was 0.3 eV in O 1s and 0.2 eV in Au 4f regions. The spectra intensity was normalized to the incident photon flux, which was measured using a Au foil. The core level binding energies (BE) were calibrated using the Fermi edge, C 1s and Au $4f_{7/2}$ second order peak. The accuracy of BE calibration was estimated to be around 0.05 eV.

All XP spectra were collected in normal photoemission mode. For quantitative XPS analysis, least-squares fitting of the spectra were performed using CasaXPS software (www.casaxps.com). A Doniach-Sunjic line shape for Au $4f_{7/2}$ and a product (multiplication) of a Gaussian with a Lorentzian line shape for O 1s with Shirley-type background were used to obtain the best fit. For surface composition calculation the cross section tables of Yeh and Lindau were used [18] and the correction for the different electron inelastic mean free pass was done using QUASES-IMFP-TPP2 M software (http://www.quases.com/products/quases-imfp-tpp2m/).

O_3 was produced using a commercial ozone generator TC-1KC. Oxygen was flowed through Teflon tubing to the ozone generator at a rate of 1 L/min. The effluent gas of the generator contained a mixture of approximately 1 % ozone and 99 % un-reacted oxygen. The O_3/O_2 mix was dosed into the experimental cell using a leak valve. O_2 and CO were dosed into the experimental cell in different ratios using mass-flow controllers (MFC) at a sample temperature of 100 °C. The total pressure in the experimental cell was 0.3 mbar.

4 Results

4.1 Au/HOPG

The first step to study the Au catalyst is to characterize the freshly prepared samples. Photoelectrons with 150 eV kinetic energy were used to collect surface sensitive Au 4f, O 1s and C 1s spectra in UHV and CO + O_2, and photons with 720 eV energy were used to collect Au 4f, O 1s and C 1s spectra during O_3 treatment (Fig. 1). Au 4f spectrum of the fresh Au/HOPG in UHV at RT [Fig. 1a(i)] shows one sharp peak at a binding energy (BE) of 83.95 eV, assigned to bulk Au in the metallic state, according to the literature [19–21]. The component shifted to low BE by the 0.3 eV is usually assigned to low-coordinated Au atoms [22]. The corresponding O 1s spectrum shows the presence of oxygen on the surface [Fig. 1b(i)]. The asymmetry of O 1s peak indicates that there is more than just one oxygen specie and the position of its maximum (BE 532.6 eV) suggests the presence of C–O, C=O and/or C–OH bonds [23, 24]. C 1s spectrum [Fig. 1c(i)] shows well-known graphite peak at BE of 284.3 eV [25].

When the O_2/O_3 mixture was introduced into the chamber and the sample was heated to 100 °C, the Au 4f spectrum changed [Fig. 1a(ii)]. A well-defined peak appears at 85.6 eV, which is assigned to an ionic Au species [21, 26]; however, with lower BE than that of Au_2O_3 (BE 85.9 eV) [27, 28]. Under O_3 the numbers of low coordinated Au atom increasing, this is evidenced by an

increase and broadening in low BE peak at 83.5 eV. According to Weststrate et al. [22] the less neighbors the lower BE, in other words an oxidation restructures Au surface and forms low-coordinated Au atoms (for example edges, kinks, etc.) on the surface. The surface sensitive O 1s spectrum [Fig. 3b(ii)] is broader in comparison with one measured in UHV. The O 1s spectrum in O_3 atmosphere consists of at least two components: the high BE species are associated with carbon–oxygen species (BE 532.6 eV) while the low BE component corresponds to oxygen on Au (BE 530.1 eV) [21, 29]. A decrease in intensity of C 1s spectrum [Fig. 1c(ii)] is due to scattering of photoelectron in gas phase.

As was shown in our previous work [30], all signs of gold oxide vanish when O_3 is evacuated from the chamber. Even an O_2-rich gas mixture ($CO/O_2 = 1:75$) does not prevent the decomposition of the oxide [Fig. 1(iii)]. In contrast to the changes found for extended Au surfaces exposed to ozone [30], the Au 4f spectral shape of Au NPs remains unchanged after O_3 treatment [Fig. 1a(iii)]. The low BE components of the Au 4f spectra does not change much, only small intensity decrease, which can be due to sintering or/and carbon accumulation [Fig. 1c(iii)]. Consistently, the peak shape of the O 1s spectrum returns to nearly the same shape as when measured in UHV, but with a slightly broader width due to the formation of new carbon–oxygen species. Note that only oxygen bonding to the carbon remains on the surface.

The quantitative analysis of surface composition is presented in Table 1. The dominant element on the surface obviously is carbon at all conditions. The amount of Au on the untreated sample is 16.5 at.%. O_3 treatment leads to oxidation of ca. 30 % of Au and significant increasing of oxygen concentration. Decreasing of Au concentration during and after O_3 treatment points out, that the sintering takes place.

Table 1 Surface composition of Au/HOPG at different conditions

	Au^0 (at.%)	Au^{3+} (at.%)	O (at.%)	C (at.%)
UHV	16.5	–	5.0	78.5
O_3	7.4	4.6	9.5	75.5
$CO + O_2$	8.0	–	10.3	81.7

The structural evolution of Au NPs during CO oxidation may help to shed light on the origin of Au activation. An SEM image of the untreated Au/HOPG is presented in Fig. 2a. The image shows Au NPs with a narrow size distribution of 6–8 nm. After O_3 treatment and CO oxidation, the Au NPs are not homogenously distributed anymore, as shown in Fig. 2b. The mean parrticle size is higher ($\sim$10 nm) than the fresh sample and some agglomerated particles are visible, which is in good agreement with quantification of the surface composition made by XPS. Burning of graphite at the interface with the Au NPs is accompanied by the migration of metallic particles on the HOPG surface (the tracks are darker in Fig. 2b). This may occur because the aggressive oxidation by O_3 leads to high mobility of Au NPs due to destruction (burning and oxidation) of carbon surface [31].

To estimate catalytic performance Au/HOPG sample was placed in the NAP-XPS chamber without any pretreatment. Then the reaction mixture ($CO:O_2 = 1:75$) was introduced to the chamber (Fig. 3a). Small fluctuations of CO flow are due to fluctuations of the MFC at very low flow. Initially, the CO_2 yield exhibits a small increase for a short time: we attribute this activity to a reaction between CO and residual O on the HOPG surface. For long time on stream, Au/HOPG does not show any significant activity under the described conditions, therefore we reason that nanostructuring is not sufficient to activate Au.

We tried to slightly oxidize Au before the reaction, using an O_3 treatment. QMS data is presented in Fig. 3b, in which Au NPs that were pre-treated with O_3 are exposed to a constant flow of a 1:75 mixture of CO and O_2. The activity of the oxidized sample is much higher than that of

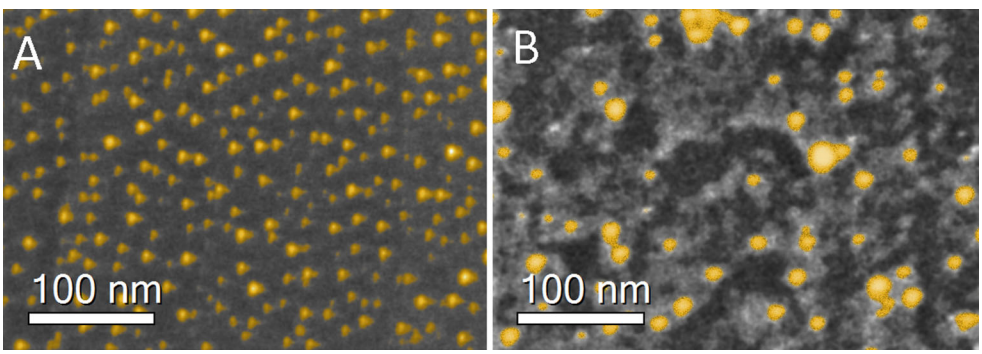

Fig. 2 SEM image of Au/HOPG **a** before and **b** after O_3 treatment at 250 °C and CO oxidation. Images were colorized in order to highlight the differences between the two samples

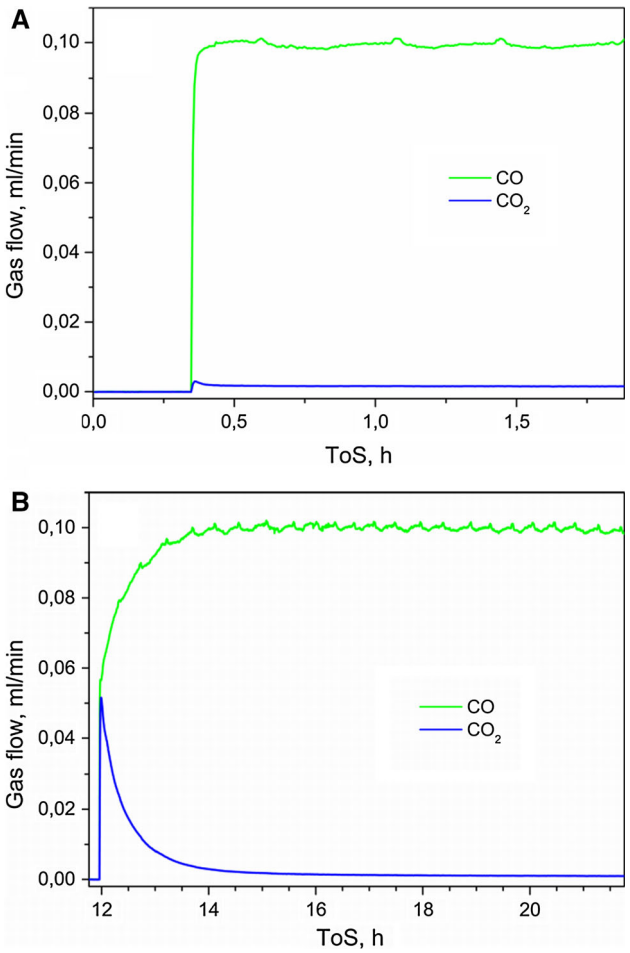

Fig. 3 QMS data of Au/HOPG **a** before and **b** after O_3 treatment at $p = 0.3$ mbar, RT and CO:O_2 = 1:75 ratio

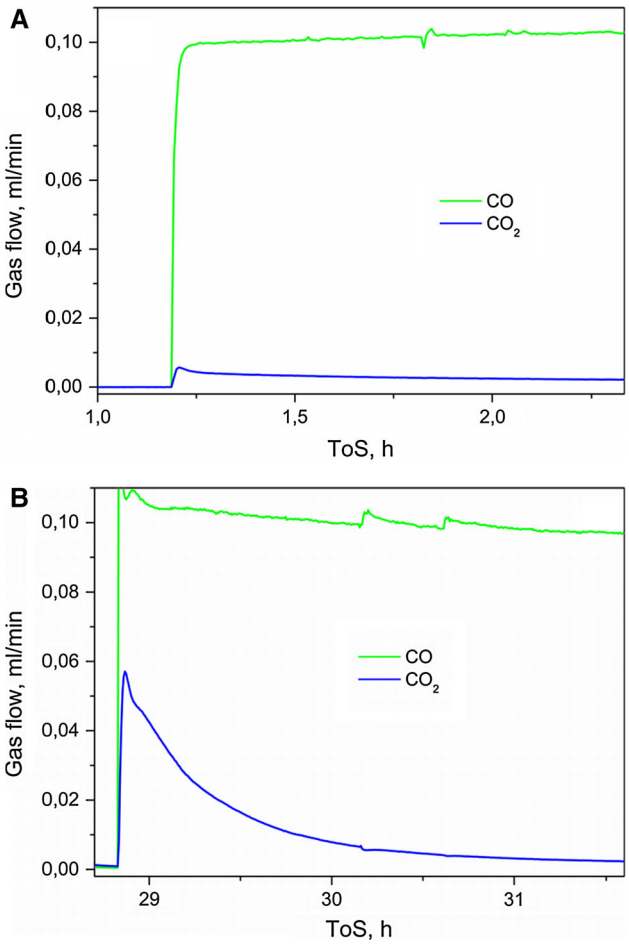

Fig. 4 QMS data of HOPG **a** before and **b** after O_3 treatment at $p = 0.3$ mbar, RT and CO:O_2 = 1:75 ratio

the sample not pre-treated with O_3, but a strong deactivation takes place, and after approximately 2 h the CO_2 yield is negligible. Thus the aglomeration does not influence the activity of Au/HOPG, suggesting that other reasons apart of the structural changes are responsible of the activation of Au. We assume that the increase of the CO_2 yield after the O_3 treatment is caused by the stoichiometric reaction between the remaining surface oxygen and CO.

4.2 Au/N-CNTs and Au/O-CNTs

Similar results were obtained for Au NPs on nitrogen- and oxygen-functionalized carbon nanotubes (Au/N-CNTs and Au/O-CNTs). The Au particle size was <5 nm. The Au NPs on functionalized CNTs consisted of a few large (ca. 40 nm diameter) particles, sparsely distributed along the tubes (not shown), along with a majority of densely dispersed nanoclusters visible only by STEM (ESI, Fig. S1). Under the same conditions, the fresh samples were inactive for CO oxidation as Au/HOPG, in spite of the significant increase of the catalyst surface area that resulted from the higher support area and Au size reduction. After O_3 treatment, Au/N-CNTs and Au/O-CNTs show the same initial activity profile as discussed for Au/HOPG and, the same rate of deactivation ($\sim$2.5 h) (not shown).

4.3 HOPG

In order to prove that stoichiometric reaction takes place, 'blank' measurements were done. A pristine HOPG crystal was placed in the sample holder and all treatment procedures were repeated. The QMS results are shown in the Fig. 4. Untreated HOPG does not catalyze the oxidation of CO as clearly shown in the Fig. 4a. However after interaction with O_3, HOPG demonstrates an initial high CO conversation that strongly decreases with time. Since HOPG contains only carbon atoms, the origin of sample's activity can be attributed only to the stoichiometric reaction between chemisorbed oxygen on the HOPG surface and CO in the gas phase.

4.4 Au/Au Foil

To further corroborate the idea that the reactivity is due to a stoichiometric reaction between CO and O functional groups on the carbon surface, we investigated Au nanoparticles supported on oxygen-free Au foil. The Au foil was chosen as a support because it is expected to be inactive in CO oxidation.

After preparation, the surface composition of the Au/Au foil is very important. All fitting parameters are given in Tables S1 and S2 in the ESI. The corresponding Au 4f spectrum [Fig. 5a(i)] of Au/Au foil shows the metallic peak at a BE of 83.95 eV with second component shifted to the low BE by 0.3 eV. This peak is assigned to the surface core-level shift [32, 33], which is ascribed mainly to the lower coordination of surface atoms compared to bulk atoms. The O 1s spectrum [Fig. 5b(i)] displays one broad peak at BE of 532.5 eV, which is in the range observed for carbonates and oxygen-containing (hydro)carbons on gold [34]. The presence of carbonates and/or oxygen-containing (hydro)carbons on the surface is confirmed by the C 1s spectrum [Fig. 5c(i)].

To clean the Au surface from the surface carbon impurities, an O_3 treatment at 150 °C was performed. When we apply the combination of high temperature (150 °C) and very reactive treatment (O_3) the carbon is burned of very rapidly, as is clearly visible in the Fig. 5c(ii). The influence of the O_3 to the sample is not limited only to the burning of the carbon, but also the oxidation of the Au surface takes place. The corresponding Au 4f spectrum [Fig. 5a(ii)] reveals the formation of Au oxide, the broad peak at BE of 85.25 eV appears under O_3 conditions, which is assigned to an ionic Au species [21, 26]. Simultaneously, a new feature in comparison with the untreated sample appears in low BE region (BE = 83.3 eV), which is assigned to the surface restructuring during oxidation [30, 35]. The O 1s spectrum Fig. 5b(ii)] has also undergone changes: the broad peak at 532.5 eV vanishes due to carbon removal and a double peak in the lower BE region is formed. The component with BE of 529.4 eV can be assigned to a surface oxide or chemisorbed oxygen on Au [29, 36, 37]; the other component (BE = 531.1 eV) has to be attributed to O in water and/or hydroxyl groups [21, 29], but also the oxidation of contaminants in concentrations below the detection limits of XPS cannot be excluded [29].

After O_3 cleaning the sample was cooled down to RT and O_3 was substituted by O_2. The cooling leads to immediate carbon accumulation as shown in the C 1s spectrum [Fig. 5c(iii)]. The high BE tail of the C 1s spectrum indicates the formation of C–O and C=O bonds on the surface during cooling in O_3 and further treatment in O_2. The O 1s spectrum in O_2 [Fig. 5b(iii)] confirms the formation of oxygen-containing (hydro)carbons on the Au

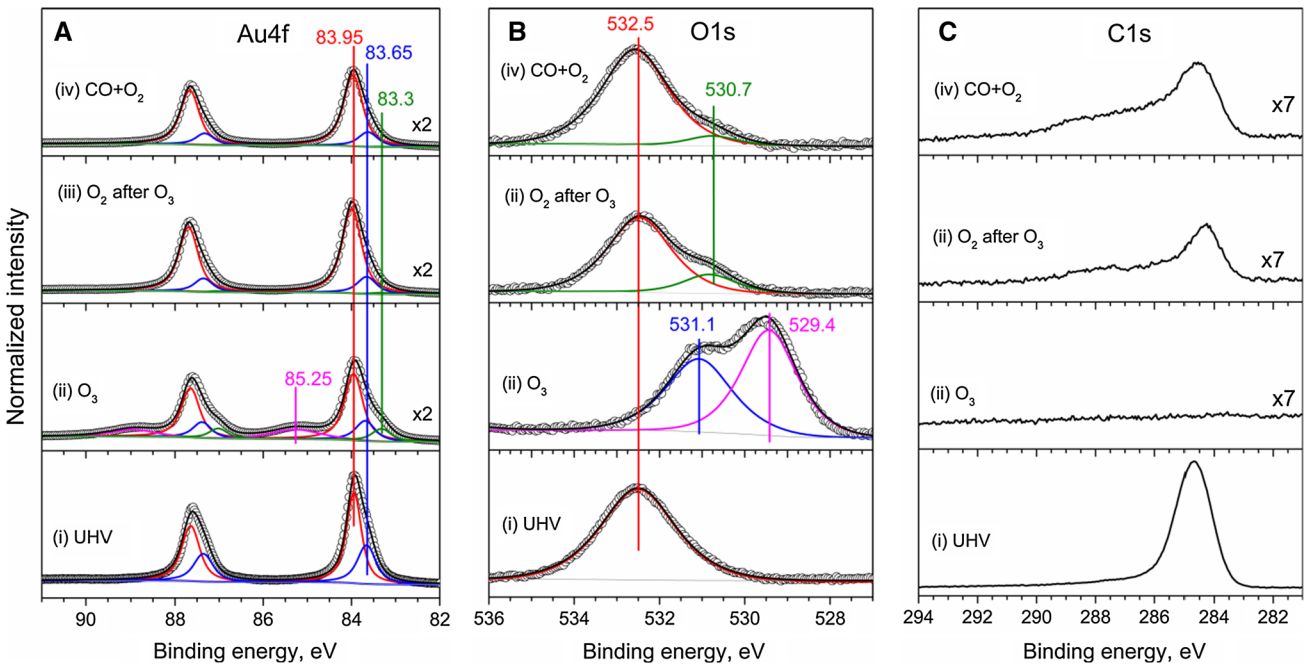

Fig. 5 NAP **a** Au 4f, **b** O 1s and **c** C 1s XP spectra of Au/Au foil (*i*) in UHV at RT, (*ii*) under O_3 at $p = 0.3$ mbar, T = 150 °C, (*iii*) under O_2 after O_3 treatment at $p = 0.3$ mbar, RT and (*iv*) under CO and O_2 atmosphere (CO:O_2 = 1:75) at $p = 0.3$ mbar, RT. Photoelectrons with 150 eV kinetic energy were used to collect surface sensitive Au 4f, O 1s and C 1s spectra in UHV, and photons with 720 eV energy were used to collect Au 4f, O 1s and C 1s spectra in O_3, O_2 and CO + O_2 atmospheres

surface, corresponding peak at 532.5 eV is well pronounced. In addition a small peak at 530.7 eV arises, and can be assigned to residual oxidized impurities in concentrations below XPS detection limit or to (hydro)carbons adsorbed on the low-coordinated atoms (defects) on the surface. There is no peak (BE < 530 eV) related to the Au oxide(s). Also no signs of Au oxide(s) (BE 85.25 eV) are in the Au 4f spectrum [Fig. 5a(iii)], but deconvolution of the spectrum shows that the peak assigned to the surface reconstruction (BE 83.3 eV) remains. Therefore, O_3 evacuation leads to decomposition of oxide(s) and carbon accumulation.

Following O_3 treatment, we introduced a reaction mixture ($CO/O_2 = 1{:}75$) into the chamber. The spectra do not change substantially. Further carbon accumulation occurs, as is seen by the increase in intensity of the C 1s peak [Fig. 5c(iv)]. The shapes of the O 1s [Fig. 5b(iv)] and Au 4f [Fig. 5a(iv)] spectra are similar in general to the ones measured in O_2 atmosphere; only the intensity of the peak (BE = 530.7 eV) corresponding to residual residual oxidized impurities with concentrations below XPS detection limit or to (hydro)carbons adsorbed on the low-coordinated atoms (defects) decreases.

Quantification of the surface composition of Au/Au foil is presented in Table 2. The untreated sample is mostly covered by carbon (69.0 at.%). Nevertheless initial considerable carbon coverage O_3 treatment cleans surface from carbon totally. Contemporaneously to carbon burning Au oxidation takes place during O_3 treatment, oxygen concentration on the surface in O_3 atmosphere exceeds stoichiometric ratio of Au_2O_3, which indicates the presence of an additional adsorbed oxygen overlayer. Changing chemical potential from O_3 to O_2 leads the decomposition of the surface oxide and fast carbon accumulation

Table 2 Surface composition of Au/Au foil at different conditions

	Au^0 (at.%)	Au^{3+} (at.%)	O (at.%)	C (at.%)
UHV	24.8	–	6.2	69.0
O_3	47.7	8.9	41.8	<1.5
O_2	37.3	–	23.4	39.3
$CO + O_2$	8	–	10.3	81.7

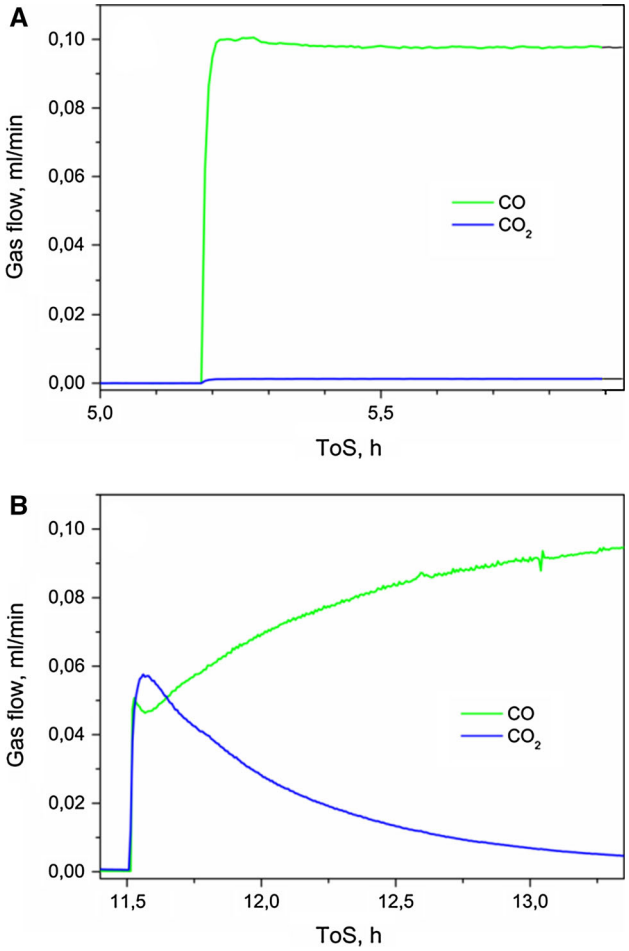

Fig. 7 QMS data of Au/Au foil **a** before and **b** after O_3 treatment at $p = 0.3$ mbar, RT and $CO{:}O_2 = 1{:}2$ ratio

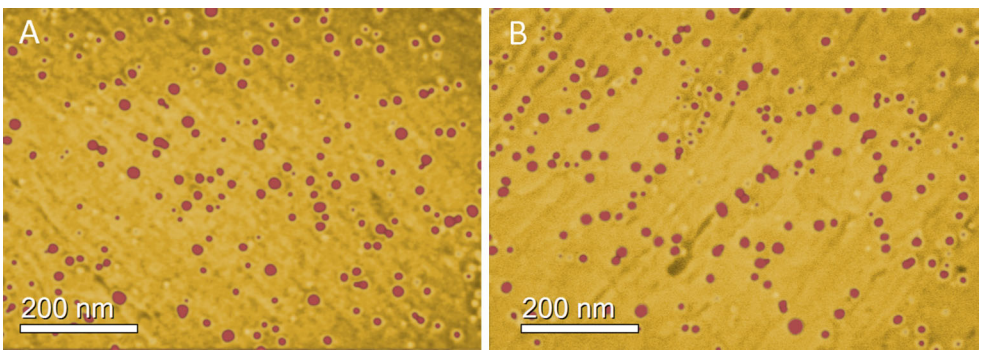

Fig. 6 SEM images of Au/Au foil **a** before and **b** after O_3 treatment. Images were colorized in order to highlight the differences between the two samples

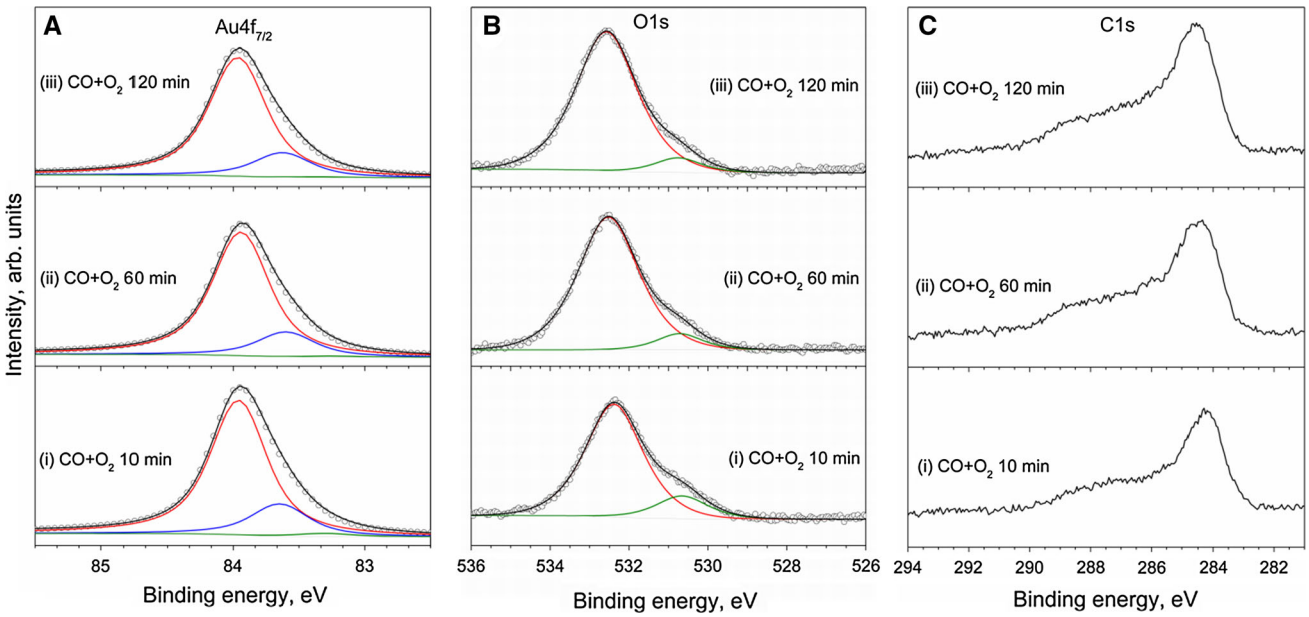

Fig. 8 NAP **a** Au 4f, **b** O 1s and **c** C 1s XP spectra of Au/Au foil under CO reaction after O_3 treatment at $p = 0.3$ mbar, RT (*i*) after 10 min, (*ii*) 60 min and (*iii*) 120 min. Photons with 720 eV energy were used to collect Au 4f, O 1s and C 1s spectra

(39.3 at.%); carbon comes from the wall of the chamber. Following CO oxidation only facilitates further increasing carbon concentration on the surface of Au/Au foil.

Microscopy does not reveal big differences between fresh and oxidized samples. SEM images of untreated Au/Au foils show a particle size of ca. 10 nm (Fig. 6a). In turn, the Au particle size distribution on O_3-treated samples shows some sintering effects and a slightly rougher surface (Fig. 6b).

A fresh electrochemically prepared sample Au/Au foil was tested under reaction conditions (Fig. 7a). The presence of the sample in the set-up does not influence the CO conversion. The CO_2 yield is negligible for the overall measurements. There are two possible explanation: (1) the adsorption of (hydro)carbons (See XPS part), which cover the surface, may prevent access of the gas mixture to the catalyst surface; or (2) Au/Au foil is an inactive catalyst. Our experiments with Au NPs ($\sim$15 nm) supported on transition metal oxides (Au/TiO_2 and Au/Fe_2O_3) in CO oxidation conducted under similar conditions show catalytic activity of the samples despite a big particle size and the presence of carbon on the surface up to 60 at.% [38], therefore surface (hydro)carbons are not relevant for inertness of Au NPs on oxygen-free supports.

However, the oxidized Au sample looks more promising, but is not stable for long times (Fig. 7b). CO consumption and deactivation time (2 h) are similar to those observed on Au/HOPG. The corresponding Au 4f, O 1s and C 1s spectra are shown in Fig. 8. In the Au 4f spectrum (Fig. 8a) the peak assigned to surface reconstruction (BE 83.3 eV) is present in a small amount. The overall intensity of the spectra decreases with time. The two components of the O 1s spectra (Fig. 8b) show opposite behavior: the oxygen-containing (hydro)carbons (BE = 532.5 eV) peak increases, while the intensity of the peak (BE = 530.7 eV) corresponding to residual residual oxidized contaminants with concentrations below XPS detection limit or to (hydro)carbons adsorbed on the low-coordinated atoms (defects) decreases during the reaction. The explanation of such behavior can be that the reaction occurs between oxidized (hydro)carbons (O_3 functionalized carbon all over the chamber) and CO molecules. When the oxygen supply is depleted the reaction stops, and carbon accumulation takes place, which is evident from increasing of C 1s peak (Fig. 8c). Thus, oxidized Au/Au foil itself does not catalyze CO oxidation at low temperature.

5 Conclusions

The results presented here indicate that Au NPs supported on oxygen-free substrates are not active catalysts in CO oxidation, unless an external source of oxygen is provided. This behavior is found to be independent of the method of preparation and the nature of the support. O_3 treatment allows cleaning of the surface, but at the same time to functionalize the carbon all over the chamber including the support. Oxygen-functionalized (hydro)carbon may still be present if their removal by O_3 treatment was not completed, and can react with CO. The stoichiometric reaction

ends rather soon after reaction initiation, and O_2 alone cannot re-functionalize the (hydro)carbons.

Under a constant chemical potential of O_3, an Au oxide is formed, but evacuation or substitution of O_3 by O_2 results in the disappearance of the surface oxide. Therefore, participation of Au oxide in CO oxidation can be excluded. Remaining low-coordinated atoms do not have sufficient catalytic properties, and CO oxidation does not occur on the Au NPs even after oxidation. Our results clearly show that the size reduction and\or the oxidation of Au is not an effective strategy to activate Au.

Acknowledgments We thank HZB for the allocation of synchrotron radiation beamtime, Gisela Weinberg (Fritz-Haber-Institute der Max-Planck, Berlin) for the SEM characterization, Manfred Schuster (Fritz-Haber-Institute der Max-Planck, Berlin) and Xing Huang (Fritz-Haber-Institute der Max-Planck, Berlin) for the TEM images and Klaus Friedel (Fritz-Haber-Institute der Max-Planck, Berlin) for sample preparation. AVB, IPP and VIB thank the Russian Science Foundation (Grant 14-23-00146) for financial support.

References

1. Haruta M, Yamada N, Kobayashi T, Iijima S (1989) J Catal 115:301–309
2. Haruta M, Tsubota S, Kobayashi T, Kageyama H, Genet MJ, Delmon B (1993) J Catal 144:175–192
3. Haruta M, Daté M (2001) Appl Catal A Gen 222:427–437
4. Hashmi ASK, Hutchings GJ (2006) Angew Chem Int Ed 45:7896–7936
5. Laguna OH, Romero-Sarria F, Centeno MA, Odriozola JA (2010) J Catal 276:360–370
6. Ryabenkova Y, He Q, Miedziak PJ, Dummer NF, Taylor SH, Carley AF, Morgan DJ, Dimitratos N, Willock DJ, Bethell D, Knight DW, Chadwick D, Kiely CJ, Hutchings GJ (2013) Catal Today 203:139–145
7. Hayashi T, Tanaka K, Haruta M (1998) J Catal 178:566–575
8. Tripathi AK, Kamble VS, Gupta NM (1999) J Catal 187:332–342
9. Bär T, Visart de Bocarmé T, Nieuwenhuys BE, Kruse N (2001) Catal Letters 74:127–131
10. Guillemot D, Borovkov VYu, Kazansky VB, Polisset-Thfoin M, Fraissard J (1997) J Chem Soc Faraday Trans 93:3587–3591
11. Boccuzzi F, Chiorino A, Manzoli M, Lu P, Akita T, Ichikawa S, Haruta M (2001) J Catal 202:256–267
12. Chen MS, Goodman DW (2004) Science 306:252–255
13. Yoon B, Häkkinen H, Landman U, Wörz AS, Antonietti J-M, Abbet S, Judai K, Heiz U (2005) Science 307:403–407
14. Minicò S, Scirè S, Crisafulli C, Visco AM, Galvagno S (1997) Catal Letters 47:273–276
15. Demidov DV, Prosvirin IP, Sorokin AM, Rocha T, Knop-Gericke A, Bukhtiyarov VI (2011) Catal Sci Technol 1:1432–1439
16. Knop-Gericke A, Kleimenov E, Hävecker M, Blume R, Teschner D, Zafeiratos S, Schlögl R, Bukhtiyarov VI, Kaichev VV, Prosvirin IP, Nizovskii AI, Bluhm H, Barinov A, Dudin P, Kiskinova M (2009) Adv Catal 52:213–272
17. Bluhm H, Hävecker M, Knop-Gericke A, Kleimenov E, Schlögl R, Teschner D, Bukhtiyarov VI, Ogletree DF, Salmeron M (2004) J Phys Chem B 108:14340–14347
18. Yeh JJ, Lindau I (1985) At Data Nucl Data Tables 32:1–155
19. Canning NDS, Outka D, Madix RJ (1984) Surf Sci 141:240–254
20. King DE (1995) J Vac Sci Technol A 13:1247–1253
21. Koslowski B, Boyen H-G, Wilderotter C, Kästle G, Ziemann P, Wahrenberg R, Oelhafen P (2001) Surf Sci 475:1–10
22. Weststrate CJ, Lundgren E, Andersen JN, Rienks EDL, Gluhoi AC, Bakker JW, Groot IMN, Nieuwenhuys BE (2009) Surf Sci 603:2152–2157
23. Desimoni E, Casella GI, Morone A, Salvi AM (1990) Surf Interface Anal 15:627–634
24. Kundu S, Wang Y, Xia W, Muhler M (2008) J Phys Chem C 112:16869–16878
25. Witek G, Noeske M, Mestl G, Shaikhutdinov S, Behm RJ (1996) Catal Lett 37:35–39
26. Tsai H, Hu E, Perng K, Chen M, Wu J-C, Chang Y-S (2003) Surf Sci 537:L447–L450
27. Juodkazis K, Juodkazyte J, Jasulaitiene V, Lukinskas A, Sebeka B (2000) Electrochem Commun 2:503–507
28. Dickinson T, Povey AF, Sherwood PMA (1975) J Chem Soc Faraday Trans 71:298–311
29. Krozer A, Rodahl M (1997) J Vac Sci Technol, A 15:1704–1709
30. Klyushin AYu, Rocha TCR, Hävecker M, Knop-Gericke A, Schlögl R (2014) Phys Chem Chem Phys 16:7881–7886
31. Tandon D, Hippo EJ, Marsh H, Sebok E (1997) Carbon 35:35–44
32. Citrin PH, Wertheim GK, Baer Y (1978) Phys Rev Lett 41:1425–1428
33. Heimann P, van der Veen JF, Eastman DE (1981) Solid State Commun 38:595–598
34. Schaefer A, Ragazzon D, Wittstock A, Walle LE, Borg A, Bäumer M, Sandell A (2012) J Phys Chem C 116:4564–4571
35. Weststrate CJ, Lundgren E, Andersen JN, Rienks EDL, Gluhoi AC, Bakker JW, Groot IMN, Nieuwenhuys BE (2009) Surf Sci 603:2152–2157
36. Saliba N, Parker DH, Koel BE (1998) Surf Sci 410:270–282
37. Min BK, Alemozafar AR, Biener MM, Biener J, Friend CM (2005) Top Catal 36:77–90
38. Klyushin AYu, Greiner MT, Huang X, Lunkenbein T, Li X, Timpe O, Friedrich M, Hävecker M, Knop-Gericke A, Schlögl R (under review) ACS Catalysis